Structural Engineering and Mechanics, *Vol. 73, No. 2 (2020) 191-207*
DOI: https://doi.org/10.12989/sem.2020.73.2.191

Free vibration analysis of FG nanoplate with poriferous imperfection in hygrothermal environment

Behrouz Karami*[1], Davood Shahsavari[1], Maziar Janghorban[1] and Li Li[2]

[1]*Department of Mechanical Engineering, Marvdasht Branch, Islamic Azad University, Marvdasht, Iran*
[2]*State Key Lab of Digital Manufacturing Equipment and Technology, School of Mechanical Science and Engineering, Huazhong University of Science and Technology, Wuhan 430074, China*

(Received July 4, 2018, Revised September 26, 2019, Accepted October 5, 2019)

Abstract. This study aims at investigating the size-dependent free vibration of porous nanoplates when exposed to hygrothermal environment and rested on Kerr foundation. Based on the modified power-law model, material properties of porous functionally graded (FG) nanoplates are supposed to change continuously along the thickness direction. The generalized nonlocal strain gradient elasticity theory incorporating three scale factors (i.e. lower- and higher-order nonlocal parameters, strain gradient length scale parameter), is employed to expand the assumption of second shear deformation theory (SSDT) for considering the small size effect on plates. The governing equations are obtained based on Hamilton's principle and then the equations are solved using an analytical method. The elastic Kerr foundation, as a highly effected foundation type, is adopted to capture the foundation effects. Three different patterns of porosity (namely, even, uneven and logarithmic-uneven porosities) are also considered to fill some gaps of porosity impact. A comparative study is given by using various structural models to show the effect of material composition, porosity distribution, temperature and moisture differences, size dependency and elastic Kerr foundation on the size-dependent free vibration of porous nanoplates. Results show a significant change in higher-order frequencies due to small scale parameters, which could be due to the size effect mechanisms. Furthermore, Porosities inside of the material properties often present a stiffness softening effect on the vibration frequency of FG nanoplates.

Keywords: free vibration; porous functionally graded materials; nonlocal strain gradient elasticity theory; hygrothermal environment; Kerr foundation

1. Introduction

The presence of size-dependent effects on mechanical characterizations of micro/nanostructures has been confirmed by experimental studies (Andrews, Gioux *et al.* 2001; Lam, Yang *et al.* 2003) as well as molecular dynamics simulation (Koh and Lee 2006). Since that the classical continuum theories were not capable to consider these effects, reconsidering of classical continuum theories when some small scale parameters are included inside their relations is introduced as an alternative way. Hence, several modified continuum theories for prediction of size-dependent effect have been proposed (see some of those in Ref. (Thai, Vo *et al.* 2017)). Nonlocal elasticity theory (NET) (Eringen and Edelen 1972) and strain gradient theory (SGT) (Lam, Yang *et al.* 2003) are just some popular models of those owing to their simplify for making comparison with those of old models without size effect (classical continuum theories). Besides that, there is a relative agreement between the results taken from NET and SGT with experimental data as well as molecular dynamics simulation in some cases (Duan, Wang *et al.* 2007; Shen, Shen *et al.* 2010; Askes and Aifantis 2011). However, the existing ratio of agreement may be not sufficient for accurate analysis in several cases. Because, the NET only provides the softening-stiffness mechanism in structures using a nonlocal parameter within Laplacian of stress, and the SGT only provides the stiffness-enhancement mechanism using the strain gradient length scale in conjunction with the Laplacian of strains, while both above mechanisms had been shown in experimental studies before. Moreover, the limitations and weaknesses of NET and SGT have been reported in some works. To cite few: the disability of NET in predicting mechanical characterization of nanobeam-like structures has been shown by (Romano, Barretta *et al.* 2017), notably those have clamped-free boundary conditions. Further, it was affirmed that the wave dispersion of nanobeams could not have been supported with those of molecular dynamics data with only NET and SGT by (Lim, Zhang *et al.* 2015) and (Li, Hu *et al.* 2015). They also investigated the applicability of nonlocal strain gradient theory (NSGT) as a single theory which obtained from a combination of NET and SGT together in wave propagation analysis. Owing to their observations, the accuracy of outcomes for all wavenumbers could be improved by implementation the NSGT instead of NET or SGT provided that an appropriate couple of small-scale parameters would be selected. In this respect, (Xiao, Li *et al.* 2017) identified a couple of nonlocal parameter and strain gradient length-scale for in-plane wave desperation of graphene with implementing classical plate theory (CPT)

*Corresponding author, Ph.D. Student
E-mail: behrouz.karami@miau.ac.ir

http://www.techno-press.com/journals/sem&subpage=7
ISSN: 1225-4568 (Print), 1598-6217 (Online)

and NSGT by applying an experimental data. In that work, the curve of wave frequency showed the priority of NSGT in comparison with NET or SGT. The results for all wave numbers improved by implementation SSDT for same analysis of wave propagation by (Karami, Shahsavari *et al.* 2018) due to the shear deformation effect in graphene sheet which it was neglected in CPT. Hence, in the current work, it is aimed to use SSDT, which is an accurate plate theory for analysis of both moderately thick and thin plates, for size-dependent vibration analysis (see in Refs. (Karami, Shahsavari *et al.* 2018; Karami, Shahsavari *et al.* 2018; Karami, Shahsavari *et al.* 2019)). On the other hand, in another work (Karami, Shahsavari *et al.* 2018), it has been shown that adding an extra nonlocal parameter into NSGT may cause to obtain better results on the response of nanoplates. This enriched model of NSGT has been called Bi-Helmholtz nonlocal strain gradient elasticity theory (B-H NSGT) (Mousavi 2016). However, the literature indicates that papers relevant to B-H NSGT for analysis of nanostructures are numerable until now. The wave propagation of double-layer nanobeams made of functionally graded materials on the basis of B-H NSGT including three distinct small-scale parameters with and without considering a thermal environment were presented by (Barati 2017; Barati and Zenkour 2017). So, as the second step to preparation of governing equations, the B-H NSGT, as a complete size-dependent theory will be considered in this paper. This theory has been considered in some works so far (Karami, Janghorban *et al.* 2017; Ebrahimi and Barati 2018; Karami, Janghorban *et al.* 2018; Karami, Janghorban *et al.* 2019; Karami, janghorban *et al.* 2019; Karami, Shahsavari *et al.* 2019).

Nowadays, functionally graded materials (FGMs) are widely used in different industries including aerospace, biomechanics, nuclear energy, optics and etc. (Miyamoto, Kaysser *et al.* 2013). In fact, the FGM is a non-uniform type of composite materials made of two or more distinct phases which their distribution regularly varies with the volume. In these materials, the metal phase usually supports a reliable mechanical performance and the ceramic phase supplies a high thermal resistance in the whole volume of FGM due to the pattern of changing in material properties of FGMs (Zemri, Houari *et al.* 2015). Hence, several models and studies have been suggested and carried out on free vibration, buckling, static, wave propagation and dynamic analysis of these materials in terms of linear and nonlinear (Mohammadi and Mahzoon 2014; Mohammadi, Mahzoon *et al.* 2014; Mehar and Panda 2016; Mahapatra, Kar *et al.* 2017; Mehar and Panda 2017; Mehar, Panda *et al.* 2017; Mehar, Panda *et al.* 2017; Mehar, Panda *et al.* 2017; Mehar, Panda *et al.* 2017; Ghayesh 2018; Ghayesh 2018; Ghayesh 2019).

During the process of FGM fabrication, voids (as known porosities) create within the materials at sintering step due to the difference in solidification temperature of material phases (Wattanasakulpong and Ungbhakorn 2014). So, it is necessary to study FGMs with porosities. As, it was proved by (Magnucki, Malinowski *et al.* 2006; Yahia, Atmane *et al.* 2015; Şimşek and Aydın 2017), the change of porosity within the thickness of porous materials leads to a variation in mechanical properties, corresponding to the pattern of

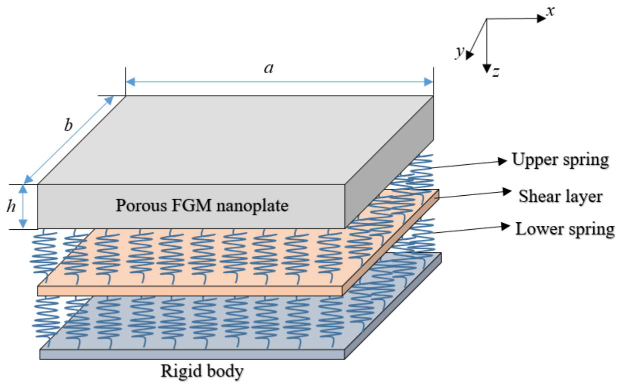

Fig. 1 Porous FGM nanoplate rested on elastic Kerr foundation.

porosity distribution. Two different patterns of porosity distributions namely even and uneven were presented in their study. (Karami, Janghorban *et al.* 2018) added a logarithmic-uneven porosity pattern into the prior patterns.

Owing to the fast progress in nanotechnology, micro/nanostructures made of FGM are often used in micro/nano-electro-mechanical systems (MEMS/NEMS) so that a large number of pioneer studies can be found in this field (Ghayesh, Amabili *et al.* 2013; Gholipour, Farokhi *et al.* 2015; Ghayesh, Farokhi *et al.* 2016). Hence, the study on porosity effect at nanoscale using size-dependent continuum theories has gained a considerable amount of interest among researchers. Some works (Mechab, Mechab *et al.* 2016; Shahverdi and Barati 2017; Karami, Shahsavari *et al.* 2018) were presented to investigate the free vibration of FGM porous nanobeams/nanoplates and it was demonstrated that the frequency increase with an increment in the volume fraction of porosity. (Shafiei, Mousavi *et al.* 2016) showed that the trend of frequency for variation of porosity volume fraction is dependent to the power-law index value. Hence, the frequency can be controlled or optimized by the variation of porosity. A similar observation was observed due to stiffness of foundation components by (Rad and Shariyat 2015). Moreover, this conclusion has been supported by (Karami, Janghorban *et al.* 2018), (Mechab, Mechab *et al.* 2016), (Wattanasakulpong and Ungbhakorn 2014), and (Atmane, Tounsi *et al.* 2017).

Certainly, there are inconsistencies in porosity effect in different conditions. Hence, frequency analysis of porous materials due to the vital role of elevated temperature and humidity of environment should be considered in the form of fundamental tasks. To cover part of this inconsistencies, in this paper, free vibration analysis of imperfect functionally graded nanoplates including porosity when exposed to a hygrothermal environment and embedded in an elastic Kerr foundation are studied using an analytic model based on the Bi-Helmholtz nonlocal strain gradient elasticity theory (B-H NSGT) and second-order shear deformation plate theory (SSDT). The B-H NSGT is applied to capture the size-dependent effects, the displacement fields of those nanoplates are derived on the basis of the SSDT. Based on the modified power-law model, material properties of porous FG rectangular nanoplates are supposed to change continuously along the thickness and three different patterns of porosity namely even, uneven and logarithmic uneven are also considered. Then, an analytical solution using Naiver series is selected to find the eigenvalue frequency.

The rest of the paper is structured as follows. Section 2 describes the material properties distribution of nonporous materials and governing equations on the basis of B-H NSGT and SSDT. Section 3 presents the eigenvalue solution method. Section 4 shows the numerical results obtained from the proposed model. Finally, remarkable conclusions derived from the study are summarized in Section 5.

2. Theoretical formulations

2.1 Porosity- and thickness-dependent material properties of FG plates

Consider an FGM nano-size plate resting on elastic Kerr foundation including porosities and a rectangular cross-section of width b and thickness h, as shown in Fig. 1. The nanoplate is composed of Al and Al_2O_3 and exposed to hygrothermal environment. The effective material properties of the nanoplate change continuously in the thickness direction of nanoplate according to a modified-power-law rule. The effective material properties $P(z)$ of porous nanoplate based on the modified rule of mixture can be expressed as (Wattanasakulpong and Ungbhakorn 2014):

$$P(z) = P_t\left(V_t - \frac{\xi}{2}\right) + P_b\left(V_b - \frac{\xi}{2}\right) \tag{1}$$

where ξ denotes the porosity coefficient (for a perfect FGM, ξ is set to zero), P_t and P_b denote the material properties of top and bottom sides, respectively; V_t and V_b are, respectively, the volume fraction of top and bottom surfaces and are related by

$$V_t + V_b = 1 \tag{2}$$

Then the volume fraction of top side is defined as follows:

$$V_t = \left(\frac{z}{h} + \frac{1}{2}\right)^k \tag{3}$$

where ($k \geq 0$) is a non-negative parameter (power-law index or the volume fraction index) which determine the material distribution across the nanoplate thickness. Based on Eqs. (1) and (2), the effective material properties of the porous FG nanoplates with even porosities are variable across the thickness direction with the following form (Wattanasakulpong and Ungbhakorn 2014):

$$E(z) = (E_t - E_b)\left(\frac{z}{h} + \frac{1}{2}\right)^k + E_b - (E_t + E_b)\frac{\xi}{2} \tag{4}$$

The hygro-thermo-elastic material properties of FG plate, including Young's modulus E, Poisson's ratio ν, thermal expansion α, moisture expansion coefficient β, shear modulus G, and mass density ρ, can be determined

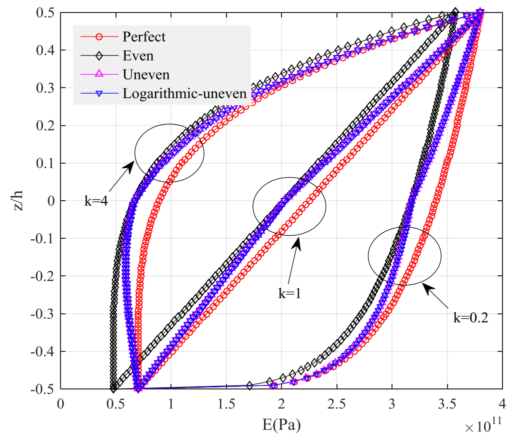

Fig. 2 Variation of Young's modulus through the thickness direction of the nanoplate considering different porosity schemes.

similarly by using Eq. (4). For uneven distribution of porosities, the effective material properties are replaced by the following form (Karami, Janghorban *et al.* 2018).

$$E(z) = (E_t - E_b)\left(\frac{z}{h} + \frac{1}{2}\right)^k + E_b - \frac{\xi}{2}(E_t + E_b)\left(1 - \frac{2|z|}{h}\right) \tag{5}$$

Also, for logarithmic-uneven distribution of porosities, the effective material properties are replaced by the following form (Karami, Janghorban *et al.* 2018).

$$E(z) = (E_t - E_b)\left(\frac{z}{h} + \frac{1}{2}\right)^k + E_b - \log\left(1 + \frac{\xi}{2}\right)(E_t + E_b)\left(1 - \frac{2|z|}{h}\right) \tag{6}$$

Using the modified power-law rule of the material property given by Eqs. (4–6), the variation of the elastic modulus through the thickness direction with the three different porosity distributions for perfect and imperfect FGMs is shown in Fig. 2. From this figure, one can easily find out that in the cases of uneven and logarithmic porosities, the moduli of elasticity equal the perfect case on the top and bottom surfaces of nanoplate, but it does not happen in the case of the even porosity.

2.2 Second-Order Shear Deformation Theory (SSDT)

According to the second order shear deformable theory, the displacement field of the FG plate can be expressed as (Khdeir and Reddy 1999)

$$u_1 = u + z\varphi_1 + z^2\varphi_2; u_2 = v + z\psi_1 + z^2\psi_2; u_3 = w \tag{7}$$

where u, v and w are mideplane displacements in the x, y and z directions, respectively; φ_i and ψ_i denote the rotation and the variables of the second-order terms. It is important to note that, the one of the advantages of SSDT is the lack of shear correction factor in the formulations. It is worth to mention that finding proper shear correction factor in some theories such as FSDT has its own difficulty in few cases. The other advantage of SSDT is the ability of modeling thick-plates accurately. The non-zero strains of the suggested plate model can be expressed as follows:

$$\begin{Bmatrix}\varepsilon_{xx}\\ \varepsilon_{yy}\\ \varepsilon_{xy}\end{Bmatrix}=\begin{Bmatrix}\dfrac{\partial u}{\partial x}\\ \dfrac{\partial v}{\partial y}\\ \dfrac{\partial u}{\partial y}+\dfrac{\partial v}{\partial x}\end{Bmatrix}+z\begin{Bmatrix}\dfrac{\partial \varphi_1}{\partial x}\\ \dfrac{\partial \psi_1}{\partial y}\\ \dfrac{\partial \varphi_1}{\partial y}+\dfrac{\partial \psi_1}{\partial x}\end{Bmatrix}+z^2\begin{Bmatrix}\dfrac{\partial \varphi_2}{\partial x}\\ \dfrac{\partial \psi_2}{\partial y}\\ \dfrac{\partial \varphi_2}{\partial y}+\dfrac{\partial \psi_2}{\partial x}\end{Bmatrix}$$
$$\begin{Bmatrix}\gamma_{xz}\\ \gamma_{yz}\end{Bmatrix}=\begin{Bmatrix}\varphi_1+\dfrac{\partial w}{\partial x}\\ \psi_1+\dfrac{\partial w}{\partial y}\end{Bmatrix}+2z\begin{Bmatrix}\varphi_2\\ \psi_2\end{Bmatrix} \tag{8}$$

Also, the extended Hamilton's principle states

$$\int_0^t \delta\left(U+V-K\right)dt=0 \tag{9}$$

where the strain energy is defined by U, the work of external loads is introduced by V and K is kinetic energy. The virtual strain energy in terms of stresses and strains is defined as follow:

$$\begin{aligned}\delta U &= \int_v \sigma_{ij}\,\delta\varepsilon_{ij}\,dV\\ &= \int_v \left[\sigma_x\delta\varepsilon_x+\sigma_y\delta\varepsilon_y+\tau_{yz}\delta\gamma_{yz}+\tau_{xz}\delta\gamma_{xz}+\tau_{xy}\delta\gamma_{xy}\right]dV\end{aligned} \tag{10}$$

Substituting Eqs. (7) and (8) into Eq. (10) yields

$$\delta U=\int_0^a\int_0^b\begin{bmatrix}N_x\dfrac{\partial\delta u}{\partial x}+M_x\dfrac{\partial\delta\varphi_1}{\partial x}+L_x\dfrac{\partial\delta\varphi_2}{\partial x}+N_y\dfrac{\partial\delta v}{\partial x}\\ +M_y\dfrac{\partial\delta\psi_1}{\partial y}+L_y\dfrac{\partial\delta\psi_2}{\partial y^2}+N_{xy}\left(\dfrac{\partial\delta u}{\partial y}+\dfrac{\partial\delta v}{\partial x}\right)\\ +M_{xy}\left(\dfrac{\partial\delta\varphi_1}{\partial y}+\dfrac{\partial\delta\psi_1}{\partial x}\right)+L_{xy}\left(\dfrac{\partial\delta\varphi_2}{\partial y}+\dfrac{\partial\delta\psi_2}{\partial x}\right)\\ +\phi_{xz}\left(\varphi_1+\dfrac{\partial w}{\partial x}\right)+\phi_{yz}\left(\psi_1+\dfrac{\partial w}{\partial y}\right)+2R_{xz}\left(\varphi_2\right)\\ +2R_{yz}\left(\psi_2\right)\end{bmatrix}dydx \tag{11}$$

where the forces and moments resultants achieved in the above equation are introduced as

$$\begin{Bmatrix}\{N\}\\ \{M\}\\ \{L\}\end{Bmatrix}=\begin{bmatrix}[A] & [B] & [C]\\ [B] & [C] & [D]\\ [C] & [D] & [E]\end{bmatrix}\begin{Bmatrix}\{\varepsilon^0\}\\ \{K\}\\ \{K'\}\end{Bmatrix}$$
$$\begin{Bmatrix}\{\phi\}\\ \{R\}\end{Bmatrix}=\begin{bmatrix}[A] & [B]\\ [B] & [C]\end{bmatrix}\begin{Bmatrix}\{\gamma^0\}\\ \{\gamma'\}\end{Bmatrix} \tag{12}$$

in which

$$(A_{ij},B_{ij},C_{ij},D_{ij},E_{ij})=\int_{-h/2}^{h/2}C_{ij}\,(1,z,z^2,z^3,z^4)dz \tag{13}$$

Note that unlike the homogeneous materials, the geometrically middle surface of heterogeneous materials (such as FG materials) may not coincide with the physically middle surface. To simplify the mechanical analyses, the physically middle surface is often adopted for quasi-static problems (Li and Hu 2017). Free vibration problems may, however, involve some errors if the physically middle surface is still adopted, see e.g., (Li and Hu 2016) for detail. In this study, the geometrically middle surface is thus used for the vibration analysis.

Next, we can define the variation of the work done by applied loads in the integral form as:

$$\delta V=\int_0^a\int_0^b\left[(N^T+N^H)\left(\frac{\partial w}{\partial x}\frac{\partial\delta w}{\partial x}+\frac{\partial w}{\partial y}\frac{\partial\delta w}{\partial y}\right)+q_{\mathrm{Kerr}}\,\delta w\right]dydx \tag{14}$$

in which N^T and N^H are related to the changes of temperature and moisture as an external loading. In fact, if we want to be realistic, all structures are exposed in hygrothermal environment so that a large number of studies have considered so far (Kar, Mahapatra *et al.* 2015; Mahapatra, Kar *et al.* 2016; Mahapatra, Panda *et al.* 2016; Mahapatra, Panda *et al.* 2016). However, in this study they are expressed as

$$\begin{aligned}N^T &= \int_{-\frac{h}{2}}^{\frac{h}{2}} E(z)\alpha(z)(\Delta T)\mathrm{d}z\\ N^H &= \int_{-\frac{h}{2}}^{\frac{h}{2}} E(z)\beta(z)(\Delta H)\mathrm{d}z\end{aligned} \tag{15}$$

In the above relations, $\Delta T=T-T_0$ and $\Delta H=H-H_0$ where T_0 and H_0 can be introduced as the reference temperature and moisture, respectively. The external transverse forces q_{Kerr} caused by elastic medium are represented in terms of displacements as (Kneifati 1985)

$$q_{\mathrm{Kerr}}-\left(\frac{k_s}{k_l+k_u}\right)\nabla^2 q_{\mathrm{Kerr}}=\left(\frac{k_l k_u}{k_l+k_u}\right)w-\left(\frac{k_s k_u}{k_l+k_u}\right)\nabla^2 w \tag{16}$$

where k_l, k_u and k_s denote the stiffness of upper and lower springs and shear layer, respectively; ∇^2 is the Laplacian operator. The variation of kinetic energy in the integral format is expressed by

$$\delta K=\int_\Omega\int_{-\frac{h}{2}}^{\frac{h}{2}}\rho(z,t)\left[\frac{\partial u_1}{\partial t}\frac{\partial\delta u_1}{\partial t}+\frac{\partial u_2}{\partial t}\frac{\partial\delta u_2}{\partial t}+\frac{\partial u_3}{\partial t}\frac{\partial\delta u_3}{\partial t}\right]dz\,d\Omega$$
$$=\int_0^a\int_0^b\begin{Bmatrix}I_0\left[\dfrac{\partial u}{\partial t}\dfrac{\partial\delta u}{\partial t}+\dfrac{\partial v}{\partial t}\dfrac{\partial\delta v}{\partial t}+\dfrac{\partial w}{\partial t}\dfrac{\partial\delta w}{\partial t}\right]\\ +I_1\left[\dfrac{\partial u}{\partial t}\dfrac{\partial\delta\varphi_1}{\partial t}+\dfrac{\partial v}{\partial t}\dfrac{\partial\delta\psi_1}{\partial t}+\dfrac{\partial\varphi_1}{\partial t}\dfrac{\partial\delta u}{\partial t}+\dfrac{\partial\psi_1}{\partial t}\dfrac{\partial\delta v}{\partial t}\right]\\ +I_2\begin{bmatrix}\dfrac{\partial u}{\partial t}\dfrac{\partial\delta\varphi_2}{\partial t}+\dfrac{\partial v}{\partial t}\dfrac{\partial\delta\psi_2}{\partial t}+\dfrac{\partial\varphi_1}{\partial t}\dfrac{\partial\delta\varphi_1}{\partial t}\\ +\dfrac{\partial\varphi_2}{\partial t}\dfrac{\partial\delta u}{\partial t}+\dfrac{\partial\psi_1}{\partial t}\dfrac{\partial\delta\psi_1}{\partial t}+\dfrac{\partial\psi_2}{\partial t}\dfrac{\partial\delta v}{\partial t}\end{bmatrix}\\ +I_3\left[\dfrac{\partial\varphi_1}{\partial t}\dfrac{\partial\delta\varphi_2}{\partial t}+\dfrac{\partial\varphi_2}{\partial t}\dfrac{\partial\delta\varphi_1}{\partial t}+\dfrac{\partial\psi_1}{\partial t}\dfrac{\partial\delta\varphi_2}{\partial t}+\dfrac{\partial\psi_2}{\partial t}\dfrac{\partial\delta\psi_1}{\partial t}\right]\\ +I_4\left[\dfrac{\partial\varphi_2}{\partial t}\dfrac{\partial\delta\varphi_2}{\partial t}+\dfrac{\partial\psi_2}{\partial t}\dfrac{\partial\delta\psi_2}{\partial t}\right]\end{Bmatrix}dydx \tag{17}$$

where

$$(I_0, I_1, I_2, I_3, I_4) = \int_{-h/2}^{h/2} \rho(z)(1, z, z^2, z^3, z^4)dz \tag{18}$$

The equilibrium equations of motion are obtained by inserting Eqs. (11-17) into Eq. (9) as follow

$$\frac{\partial N_{xx}}{\partial x} + \frac{\partial N_{xy}}{\partial y} = I_0 \frac{\partial^2 u}{\partial t^2} + I_1 \frac{\partial^2 \varphi_1}{\partial t^2} + I_2 \frac{\partial^2 \varphi_2}{\partial t^2} \tag{19}$$

$$\frac{\partial N_{yy}}{\partial y} + \frac{\partial N_{xy}}{\partial x} = I_0 \frac{\partial^2 v}{\partial t^2} + I_1 \frac{\partial^2 \psi_1}{\partial t^2} + I_2 \frac{\partial^2 \psi_2}{\partial t^2} \tag{20}$$

$$\frac{\partial \phi_{xz}}{\partial x} + \frac{\partial \phi_{yz}}{\partial y} - q_{\text{Kerr}} - (N^T + N^H)\nabla^2 w = I_0 \frac{\partial^2 w}{\partial t^2} \tag{21}$$

$$\frac{\partial M_{xx}}{\partial x} + \frac{\partial M_{xy}}{\partial y} - \phi_{xz} = I_1 \frac{\partial^2 u}{\partial t^2} + I_2 \frac{\partial^2 \varphi_1}{\partial t^2} + I_3 \frac{\partial^2 \varphi_2}{\partial t^2} \tag{22}$$

$$\frac{\partial L_{xx}}{\partial x} + \frac{\partial L_{xy}}{\partial y} - 2R_{xz} = I_2 \frac{\partial^2 u}{\partial t^2} + I_3 \frac{\partial^2 \varphi_1}{\partial t^2} + I_4 \frac{\partial^2 \varphi_2}{\partial t^2} \tag{23}$$

$$\frac{\partial M_{yy}}{\partial y} + \frac{\partial M_{xy}}{\partial x} - \phi_{yz} = I_1 \frac{\partial^2 v}{\partial t^2} + I_2 \frac{\partial^2 \psi_1}{\partial t^2} + I_3 \frac{\partial^2 \psi_2}{\partial t^2} \tag{24}$$

$$\frac{\partial L_{yy}}{\partial y} + \frac{\partial L_{xy}}{\partial x} - 2R_{yz} = I_2 \frac{\partial^2 v}{\partial t^2} + I_3 \frac{\partial^2 \psi_1}{\partial t^2} + I_4 \frac{\partial^2 \psi_2}{\partial t^2} \tag{25}$$

2.3 Bi-Helmholtz nonlocal strain gradient elasticity model for FG nanoplates

To show the size dependency of vibration behavior, the higher order of nonlocal strain gradient theory can be used and the stress can be expressed by:

$$\sigma_{ij} = \sigma_{ij}^{(0)} - \nabla \sigma_{ij}^{(1)} \tag{26}$$

where stress $\sigma_{ij}^{(0)}$ corresponds to strain ε_{ij} and higher-order stress $\sigma_{ij}^{(1)}$ correspondents to strain gradient $\nabla \varepsilon_{ij}$ and the stress can be written as follows

$$\begin{aligned} \sigma_{ij}^{(0)} &= \int_V Q_{ijkl}\, \alpha_0 \left(x, x', e_0 a\right) \varepsilon'_{kl}(x')dx' \\ \sigma_{ij}^{(1)} &= l^2 \int_V Q_{ijkl}\, \alpha_1 \left(x, x', e_1 a\right) \nabla \varepsilon'_{kl}(x')dx' \end{aligned} \tag{27}$$

in which Q_{ijkl} are the elastic constants; α_0 is the kernel function corresponding to the strain field; and α_1 is the kernel function corresponding to the strain gradient field. e_0a and e_1a consider the influence of nonlocal stress field, a is an internal characteristic length; l is the strain gradient length-scale parameter and captures the effects of higher-order strain gradient stress field. According to this fact that solving differential equations is easier than integral equations, Lim *et al*. (Lim, Zhang *et al*. 2015) introduced a general and extended constitutive equation for the higher-order nonlocal strain gradient theory as

$$\begin{aligned} &\left[1 - \mu_1^2 \nabla^2\right]\left[1 - \mu_0^2 \nabla^2\right]\sigma_{ij} = Q_{ijkl}\left[1 - \mu_1^2 \nabla^2\right]\varepsilon_{kl} \\ &- Q_{ijkl}\, l^2 \left[1 - \mu_0^2 \nabla^2\right]\nabla^2 \varepsilon_{kl} \end{aligned} \tag{28}$$

in which

$$\mu_0 = e_0 a, \mu_1 = e_1 a \tag{29}$$

By choosing $\mu_0 = \mu_1 = \mu$, Eq. (28) can be written in a simpler form for lower-order nonlocal strain gradient constitutive relation. That is,

$$\left[1 - \mu^2 \nabla^2\right]\sigma_{ij} = Q_{ijkl}\left[1 - l^2 \nabla^2\right]\varepsilon_{kl} \tag{30}$$

The following equation can be used to include the influences of hygro-thermal loading in the Eq. (33) (Karami, Shahsavari *et al*. 2018)

$$\begin{aligned} &\left(1 - \mu_1^2 \nabla^2\right)\left(1 - \mu_0^2 \nabla^2\right)\sigma_{ij} \\ &= Q_{ijkl}\left[\left(1 - \mu_1^2 \nabla^2\right)\varepsilon_{kl} - l^2\left(1 - \mu_0^2 \nabla^2\right)\nabla^2 \varepsilon_{kl} - \alpha_{ij}\Delta \mathrm{T} - \beta_{ij}\Delta \mathrm{H}\right] \end{aligned} \tag{31}$$

where α_{ij} and β_{ij} are thermal and moisture expansion coefficients, respectively; T and H are the temperature and moisture variation, respectively. The equivalent form of Eq. (36) is presented as

$$\mathcal{L}_\mu \sigma_{ij} = Q_{ijkl}\left[\mathcal{L}_l \varepsilon_{kl} - \alpha_{ij}\Delta \mathrm{T} - \beta_{ij}\Delta \mathrm{H}\right] \tag{32}$$

where the linear operators are defined as

$$\begin{aligned} \mathcal{L}_\mu &= (1 - \mu_1^2 \nabla^2)(1 - \mu_0^2 \nabla^2) \\ \mathcal{L}_l &= (1 - \mu_1^2 \nabla^2) - l^2(1 - \mu_0^2 \nabla^2)\nabla^2 \end{aligned} \tag{33}$$

2.4 Governing equations of nonlocal strain gradient theory

The equilibrium equations in terms of the displacements of the NSGT in conjunction with SSDT for FGM nanoplate can be derived by substituting Eq. (12) into Eqs. (19)-(25). These obtained equations can be found in Appendix.

3. Solution method

Since the order of the size-dependent governing equations is higher than that of the classical equations, one should find new (non-classical) boundary conditions to solve governing equations. Best method for finding the boundary conditions may be Hamilton's principle, which is difficult in the presence of nonlocal strain gradient theory. In this suggestion, we assume an analytical solution for our governing equations (just like Navier method) and then we compared our results with the results of researches including non-classical boundary conditions. If our results have good agreement with them, it may be concluded that the suggested series can be a good method for approximating the non-classical boundary conditions. Therefore, we have the permission to use them for solving governing equations. Considering simply supported boundary condition, the following series are suggested.

$$u=\sum_{n=1}^{\infty}\sum_{m=1}^{\infty}U_{mn}e^{-i\omega_{mn}t}\cos\alpha x\sin\beta y$$
$$v=\sum_{n=1}^{\infty}\sum_{m=1}^{\infty}V_{mn}e^{-i\omega_{mn}t}\sin\alpha x\cos\beta y$$
$$w=\sum_{n=1}^{\infty}\sum_{m=1}^{\infty}W_{mn}e^{-i\omega_{mn}t}\sin\alpha x\sin\beta y$$
$$\varphi_1=\sum_{n=1}^{\infty}\sum_{m=1}^{\infty}\Phi_{1mn}e^{-i\omega_{mn}t}\cos\alpha x\sin\beta y \quad (34)$$
$$\varphi_2=\sum_{n=1}^{\infty}\sum_{m=1}^{\infty}\Phi_{2mn}e^{-i\omega_{mn}t}\cos\alpha x\sin\beta y$$
$$\psi_1=\sum_{n=1}^{\infty}\sum_{m=1}^{\infty}\Psi_{1mn}e^{-i\omega_{mn}t}\sin\alpha x\cos\beta y$$
$$\psi_2=\sum_{n=1}^{\infty}\sum_{m=1}^{\infty}\Psi_{2mn}e^{-i\omega_{mn}t}\sin\alpha x\cos\beta y$$

where $i=\sqrt{-1}$; $\alpha=m\pi/a$; $\beta=n\pi/b$; m and n are the half wave numbers for x and y directions, respectively. The simply supported boundary conditions for the rectangular nanoplate are

$$u=w=\psi_1=\psi_2=N_{xx}=M_{xx}=0 \text{ at } x=0,a \quad (35)$$

$$v=w=\varphi_1=\varphi_2 N_{yy}=M_{yy}=L_{xy}=0 \text{ at } y=0,b \quad (36)$$

Using Eq. (41), the simply supported boundary conditions for the nanoplates, i.e., Eqs. (42) and (43), will be satisfied automatically. By substituting Eq. (34) into the appendix's equations, we obtain the linear equation system

$$([K]_{7\times7}-\omega_{mn}^2[M]_{7\times7})\{\Delta\}=\{0\} \quad (37)$$

in which $\Delta=\{U_{mn},V_{mn},W_{mn},\Phi_{1mn},\Phi_{2mn},\Psi_{1mn},\Psi_{2mn}\}^T$. $[K]$ represents the stiffness matrix and $[M]$ denote the mass matrix. Eq. (44) is a standard eigenvalue problem where the eigenvalues are found by setting the determinant of ($[K]$-$\omega_{mn}^2[M]$) to zero. The smallest eigenvalues are the dominant natural frequency of the system.

4. Solution method

In this section, vibration response of nanosize plates made of FGMs with three different types of porosity patterns (namely even, uneven, and logarithmic-uneven patterns) is investigated based on a NSGT and SSDT. Also, it is assumed that the nanoplate is rested on Kerr foundation and exposed to the hygrothermal environment. In this study, various non-dimensional parameters are used as follows:

$$\tilde{\omega}=\omega h\sqrt{\rho_m/E_m},\mathrm{K}_l=\frac{k_l a^4}{D_{11}},\mathrm{K}_u=\frac{k_u a^4}{D_{11}}$$

$$\mathrm{K}_s=\frac{k_s a^2}{D_{11}},\text{ and } D_{11}=(E_m h^3)/(12(1-\nu_m^2))$$

The length of nanoplate is considered as a=10 nm. As mentioned, the material properties of FGMs are dependent on the porosities. Material properties of FG nanoplate are listed in Table 1. Table 2 presents the verification of the non-dimensional frequency of a rectangular nanoplate of simply-supported boundary condition with that presented by Aghababaei and Reddy (Aghababaei and Reddy 2009) using third-order shear deformation theory (TSDT). In this table, the frequencies are in a good agreement for the different values of length-to-width and length-to-thickness ratios and nonlocal parameters.

In Table 3 the non-dimensional frequencies of Al/Al_2O_3 FG square plates are computed for different power-law indices and length-to-thickness ratios a/h. They are compared with the 3D-exact solutions of Jin *et al*. (Jin, Su *et al*. 2014). Again, the present results are in good agreement with these solutions.

Table 4 contains the first three non-dimensional frequencies of Al/Al_2O_3 FG square plate with respect to

Table 1 Material properties of the used (Al/Al_2O_3) FG nanoplate

Material	E (GPa)	ρ (kg/m^3)	ν	α (/K)	β (wt.%H$_2$O)$^-$
Al	70	2702	0.3	23×10^{-6}	0.44
Al_2O_3	380	3800	0.3	7×10^{-6}	0.001

Table 2 Comparison of first non-dimensional frequency $\hat{\omega}_{11}=\omega_{11}h\sqrt{\rho/G}$ of S-S rectangular plates (a=10nm, E=30×10^{6}Pa, ρ=2750kg/m^3, ν=0.3)

			μ (nm)		
b/a	a/h	Method	0	1	2
1	10	Present	0.0934	0.0854	0.0702
		TSDT*	0.0963	0.0880	0.0720
	20	Present	0.0239	0.0218	0.0179
		TSDT*	0.0241	0.0220	0.0180
2	10	Present	0.0591	0.0557	0.0484
		TSDT*	0.0602	0.0563	0.0493
	20	Present	0.0150	0.0141	0.0123
		TSDT*	0.0150	0.0142	0.0123

*TSDT: Ref. (Aghababaei and Reddy 2009)

Table 3 Comparison of non-dimensional frequencies $\tilde{\omega}=\omega h\sqrt{\rho_m/E_m}$ of Al/Al_2O_3 FG square plates, (a=10, b/a=1, a/h=10)

			k	
a/h	Method	0	1	2
10	Present	0.1138	0.0871	0.0790
	3D exact*	0.1135	0.0870	0.0789
5	Present	0.4209	0.3234	0.2921
	3D exact*	0.4169	0.3222	0.2905
2	Present	1.9004	1.4876	1.3302
	3D exact*	1.8470	1.4687	1.3095

*3D exact: Ref. (Jin, Su *et al*. 2014)

Table 4 Comparison of non-dimensional frequencies $\bar{\omega}=(\omega/h)\sqrt{\rho_c/E_c}$ of Al/Al_2O_3 FG square plates, (a/h=10, b/a=1, $\mu_0=\mu_1=l=0$)

		k				
Mode	Method	0	0.5	1	4	10
(1,1)	Present	0.0579	0.0492	0.0443	0.0383	0.0367
	Quasi-3D*	0.0578	0.0494	0.0449	0.0389	0.0369
(1,2)	Present	0.1390	0.1182	0.1066	0.0914	0.0874
	Quasi-3D*	0.1381	0.1185	0.1077	0.0923	0.0868
(2,2)	Present	0.2142	0.1826	0.1646	0.1404	0.1340
	Quasi-3D*	0.2123	0.1827	0.1660	0.1410	0.1320

*Quasi- 3D: Ref. (Farzam-Rad, Hassani *et al*. 2017)

Table 5 Comparison of non-dimensional frequency $\hat{\omega}=\omega a^2/h\sqrt{\rho_m/E_m}$ for porous plate with different distribution type of porosities, (b/a=1, k=1, ξ=0.2, $\mu_0=\mu_1=l=0$)

h/a	Method	Even	Uneven	Logarithmic-uneven
0.1	Exact*	8.248	8.781	8.815
	Quasi-3D*	8.203	8.845	8.843
	Present	8.2446	8.7890	8.7853
0.2	Exact*	7.675	8.097	8.094
	Quasi-3D*	7.641	8.164	8.163
	Present	7.6837	8.1388	8.1365

*Exact: Ref. (Zhao, Choe *et al*. 2018); *Quasi-3D: Ref. (Shahsavari, Shahsavari *et al*. 2018)

different power-law indices. It is obvious that the results of present model have very good compliance with the available literature (Farzam-Rad, Hassani *et al*. 2017).

Table 5 presents a comparison between the results of present formulation and those of (Zhao, Choe *et al*. 2018) and (Shahsavari, Shahsavari *et al*. 2018) reported for porous FGMs using 3D- elasticity theory and a higher-order refined plate, respectively. As can be seen, a good agreement is achieved between the theories especially for thick plates.

Also, as the last step of comparison section, non-dimensional frequencies of a higher-order nonlocal strain gradient rectangular nanoplates are compared with higher-order nonlocal strain gradient shear deformation model of (Nematollahi, Mohammadi *et al*. 2017) for different lower-order and higher-order nonlocal parameters and strain gradient length scale parameter in Table 6. It can be seen that all the obtained results are in an excellent agreement with other available solutions, thus the proposed formulation possesses sufficient accuracy and reliability for prediction about the free vibration response of FG nanoplates.

One of the main aims of this study is to provide the vibration response of simply supported FG nanosize plates with respect to nonlocal parameters and strain gradient length scale parameter. So, as a benchmark table, vibration response of FG nanosize plate for the first-order non-dimensional natural frequency for different nonlocal parameters, strain gradient length scale, aspect ratio (a/b) and thickness of the plate has been tabulated in Table 7. As can be seen, the non-dimensional natural frequency of FG nanoplate rises with the increment of the strain gradient length scale and reduces with the increment of the nonlocal parameters.

Relying on the results obtained from this table for various amounts of higher-order nonlocal parameter, we can conclude that in the case that the strain gradient length scale is zero, the variations of the higher-order nonlocal parameter will be inefficient. In other words, it can be concluded that raising the lower-order nonlocal parameter at small amounts of the strain gradient length scale has more effects on reducing the non-dimensional natural frequency of FG nanoplate, compared with raising the higher-order nonlocal parameter. Nevertheless, raising the higher-order nonlocal parameter at large amounts of the strain gradient length scale has more effects on reducing the natural frequency, compared with raising the lower-order nonlocal parameter. In order to better understanding of this issue, the first three non-dimensional natural frequencies of the FG nanoplate have been illustrated in Fig. 3 with respect to raising the strain gradient length scale and various values of nonlocal parameters when (k=1, a/h=100, b/a=1, ξ=0).

For different values of nonlocal parameters, Fig. 4 plots the variations of the first three non-dimensional natural frequencies of the FG nanoplate as a function of scale factor (C_1), where

$$C_1=l\backslash\mu,\ \mu_0=\mu_1=\mu$$

It is easily observable that when the scale factor is less than unity, the nanoplate provides softer response and the size-dependent natural frequencies are smaller than those from classical model. For C_1=1, the achieved frequencies are the same as those determined by classical solution. Moreover, for the values of nonlocal parameter smaller than gradient parameter, the frequencies achieved from present theory are larger than those from the classical model. Besides, further changes can be seen in higher order frequencies with the variation of the scale factor. Moreover, it should be noted that by ignoring the scale factor, the obtained results are equal to those from Eringen's nonlocal theory.

Variations for the first three non-dimensional frequencies of FG nanoplate due to differences in small-scale parameters is presented in Fig. 5. A new scale factor (C_2) has been applied to study the trend of natural frequency in FG nanoplate as follows

$$C_2=l\backslash\mu_1,\ \mu_0=C_2$$

It is clear that by taking various values of small-scale parameters, the different variations in the responses of natural frequency for FG nanoplates could be seen. In some cases, the frequency rises by raising the scale factor, while in some other cases the frequency reduces according to increase of the scale factor. Besides, with considering some different values for higher-order nonlocal parameter, with

Table 6 Comparison of non-dimensional frequencies of simply supported rectangular nanoplate. (a=10 nm, a/h=50, b/a=1)

			l (nm)					
μ_0 (nm)	μ_1 (nm)	Method	0	1	2	3	4	5
	0	Present	0.00352	0.00391	0.00490	0.00352	0.00769	0.00924
		CPT*	0.00352	0.00391	0.00491	0.00623	0.00770	0.00925
1	1	Present	0.00352	0.00385	0.00470	0.00586	0.00717	0.00857
		CPT*	0.00352	0.00385	0.00471	0.00587	0.00718	0.00858
	2	Present	0.00352	0.00374	0.00435	0.00520	0.00620	0.00729
		CPT*	0.00352	0.00375	0.00435	0.00521	0.00621	0.00730
2	0	Present	0.00288	0.00335	0.00447	0.00588	0.00742	0.00902
		CPT*	0.00288	0.00335	0.00447	0.00589	0.00743	0.00903
	1	Present	0.00288	0.00327	0.00425	0.00550	0.00688	0.00832
		CPT*	0.00288	0.00328	0.00425	0.00551	0.00689	0.00833
	2	Present	0.00288	0.00315	0.00385	0.00479	0.00587	0.00701
		CPT*	0.00288	0.00315	0.00385	0.00480	0.00587	0.00701

*CPT: Ref. (Nematollahi, Mohammadi *et al*. 2017)

Table 7 First non-dimensional frequency of S-S porous nanoplate, (a=10nm, k=1)

					l (nm)			
a/h	μ_0 (nm)	μ_1 (nm)	0	1	2	3	4	5
20	0	0	0.02223	0.02433	0.02974	0.03704	0.04533	0.05416
		1	0.02223	0.02340	0.02863	0.03503	0.04240	0.05031
		2	0.02223	0.02342	0.02669	0.03138	0.03696	0.04309
	1	0	0.02032	0.02259	0.02834	0.03593	0.04442	0.05340
		1	0.02032	0.02223	0.02718	0.03385	0.04143	0.04949
		2	0.02032	0.02162	0.02512	0.02516	0.03585	0.04214
	2	0	0.01662	0.01933	0.02581	0.03397	0.04286	0.05211
		1	0.01662	0.01891	0.02454	0.03177	0.03975	0.04809
		2	0.01662	0.01818	0.02223	0.02769	0.03388	0.04048
50	0	0	0.00358	0.00392	0.00479	0.00596	0.00730	0.00872
		1	0.00358	0.00386	0.00461	0.00564	0.00683	0.00810
		2	0.00358	0.00377	0.00430	0.00505	0.00595	0.00694
	1	0	0.00327	0.00364	0.00456	0.00578	0.00715	0.00860
		1	0.00327	0.00357	0.00438	0.00545	0.00667	0.00797
		2	0.00327	0.00348	0.00404	0.00484	0.00577	0.00678
	2	0	0.00268	0.00311	0.00416	0.00547	0.00690	0.00839
		1	0.00268	0.00304	0.00395	0.00511	0.00640	0.00774
		2	0.00268	0.00293	0.00358	0.00446	0.00546	0.00652

the increase of scale factor, the natural frequency initially decrease and then it is increased at higher intervals. Obviously, similar trends of movement for other modes of vibration can be seen with respect to different small-scale parameters.

As another study, to better understanding the vibration response of FG nanoplate in hygrothermal environment Figs. 6 and 7 are plotted under uniform temperature and moisture rise. Variations of first two natural frequencies of a FG nanosize plate with respect to nonlocal parameters and various values of temperature differences at (k=1, a/h=10, b/a=1, l=1nm, ξ=0) have been demonstrated in Fig. 6. As we can see in figure, an increase in the temperature causes to a decrease in natural frequencies of the FG nanosize plate.

In Fig. 7 we study the effects of evaluating moisture with respect to nonlocal parameters on the first two natural frequencies of FG nanosize plate when (k=1, a/h=10, b/a=1, l=1nm, ξ=0). It is evident that the vibration natural frequencies become smaller as the moisture difference increases for all nonlocal parameters.

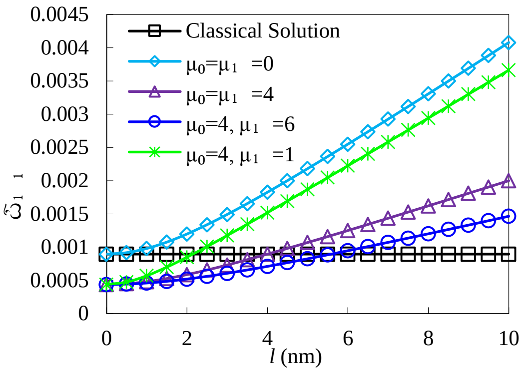

(a) First non-dimensional natural frequency

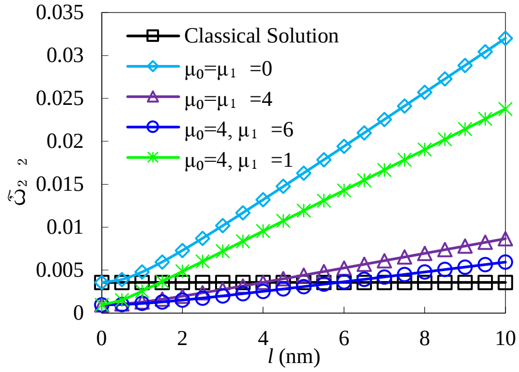

(b) Second non-dimensional natural frequency

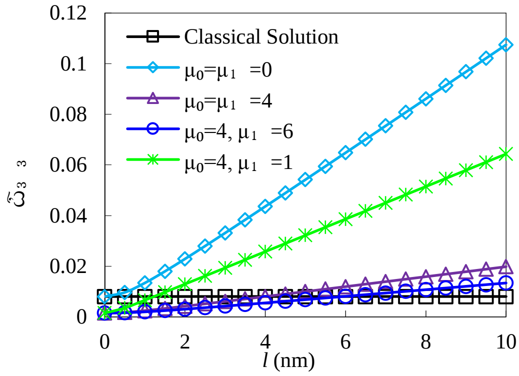

(c) Third non-dimensional natural frequency

Fig. 3 Variations of the first three non-dimensional natural frequencies of simply supported FG nanoplate versus power-law index with respect to strain gradient length scale and nonlocal parameters

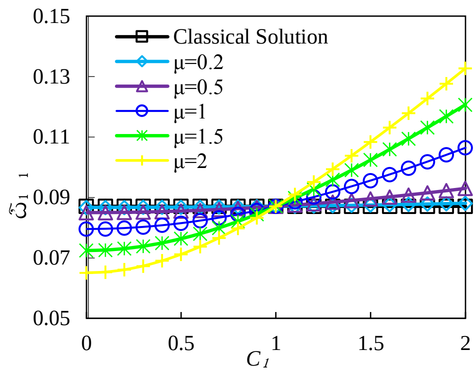

(a) First non-dimensional natural frequency

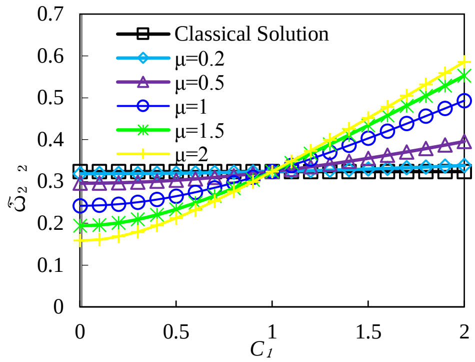

(b) Second non-dimensional natural frequency

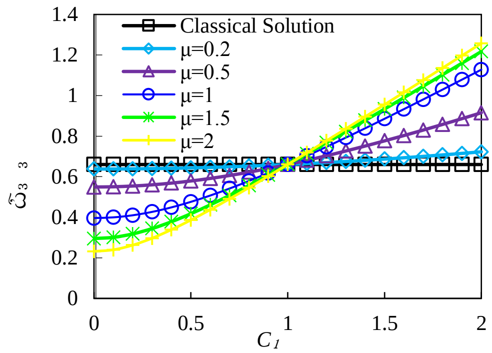

(c) Third non-dimensional natural frequency

Fig. 4 Variations of the first three non-dimensional natural frequencies of the rectangular simply supported FG nanoplate with respect to scale factor (C_1) and nonlocal parameter (μ)

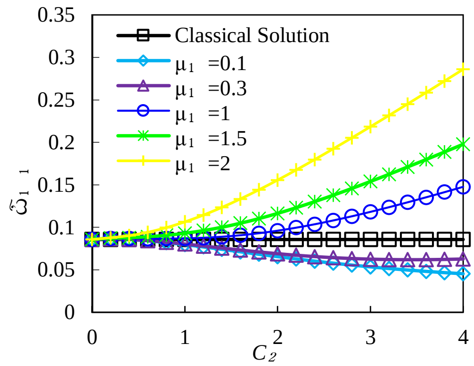

(a) First non-dimensional natural frequency

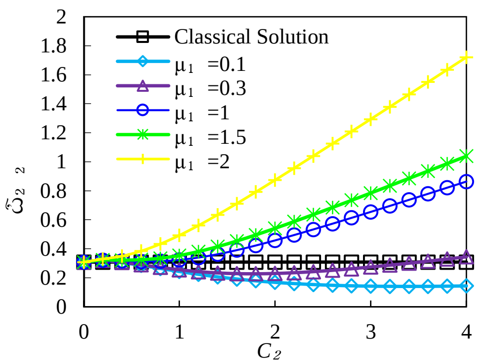

(b) Second non-dimensional natural frequency

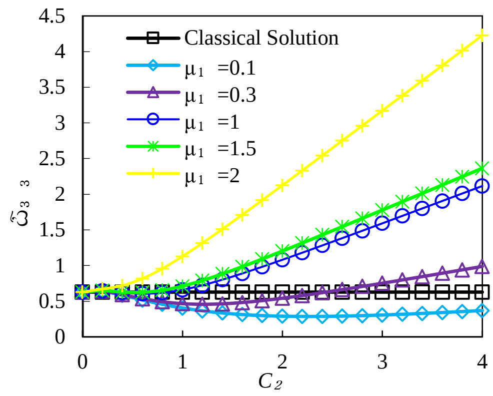

(c) Third non-dimensional natural frequency

Fig. 5 Variations of the first three non-dimensional natural frequencies of the rectangular simply supported FG nanoplate with respect to scale factor (C_2) and higher-order nonlocal parameter (μ_1)

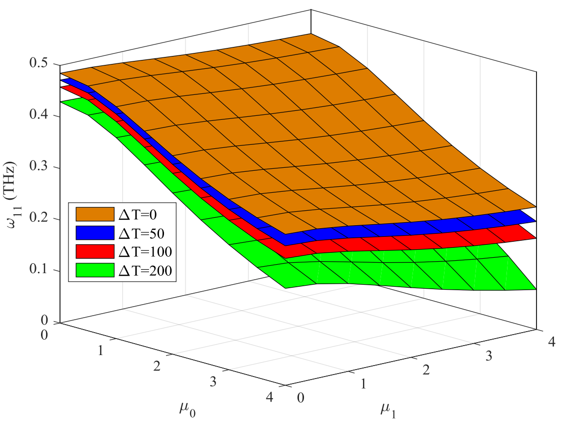

(a) First non-dimensional natural frequency

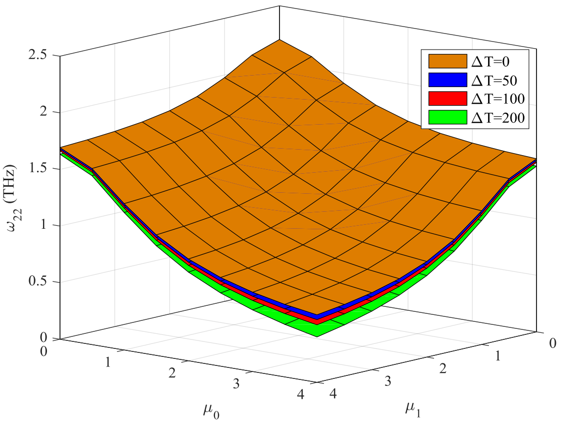

(b) Second non-dimensional natural frequency

Fig. 6 Variations of first two natural frequencies of a simply supported FG nanoplate under uniform temperature rise with respect to nonlocal parameters at fixed gradient length scale

Furthermore, from Figs. 6 and 7 it is clearly observable that inclusion of nonlocal parameters has a stiffness-hardening impact on the FG nanoplate structure. It is also

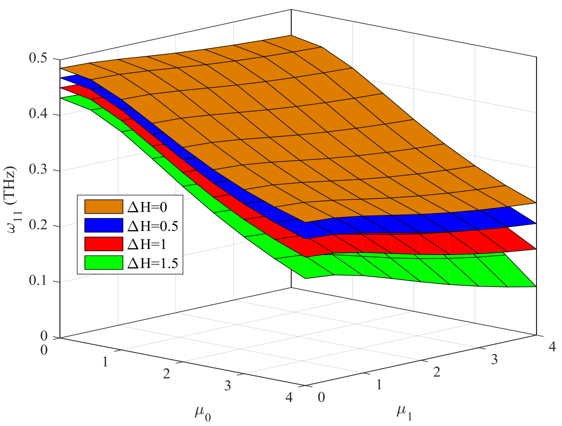

(a) First non-dimensional natural frequency

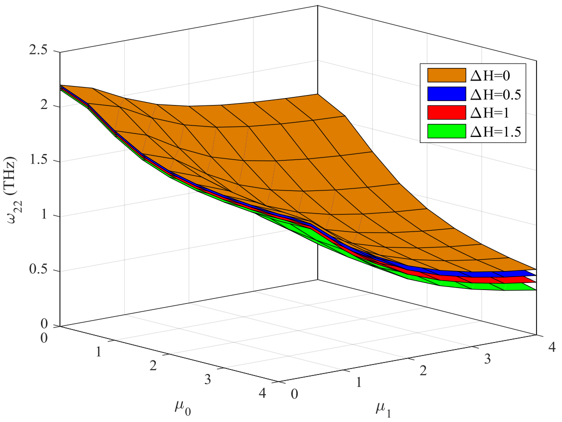

(b) Second non-dimensional natural frequency

Fig. 7 Variations of first two natural frequencies of a simply supported FG nanoplate under uniform moisture rise with respect to nonlocal parameters at fixed gradient length scale

seen that natural frequencies of the FG nanoplate are significantly affected by the moisture and temperature differences, especially at high values of nonlocal parameter.

Table 8 presents first non-dimensional natural frequency of FG nanosize plates, which figures out the effect of aspect ratio (varying from 1 to 2), length-to-thickness ratio (varying from 2 to 50), power-law index (varying from 0.2 to 5) and three different types of porosity changes (varying from 0 to 0.2) for nonlocal parameters $\mu_0=\mu_1=2$nm and strain gradient length scale $l=1$nm. As it is seen in Table 8, results decreasing in the natural frequency, due to increases in ceramics phase constituent, and hence, the stiffness of the plate. However, a growth in aspect ratio and length-to-thickness ratio cause to decrease in natural frequency, at all power-law index. In addition, it is seen that the variation of first non-dimensional natural frequency by employing all type of porosities occurs in different ways and this phenomenon depends on the composition of the material. This may be related to the concentrated of nanovoids inside FG plate.

To the more accurate analysis of vibration response, the first three non-dimensional natural frequencies of porous

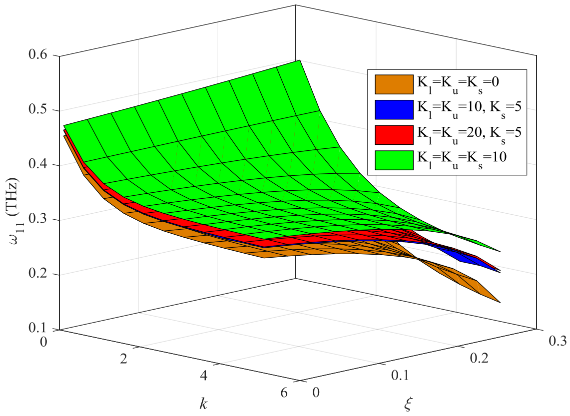

(a) First non-dimensional natural frequency

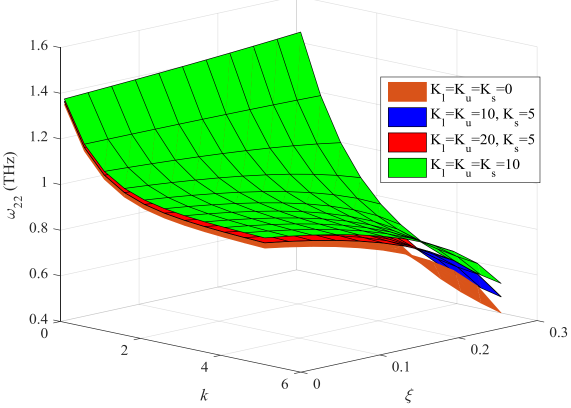

(b) Second non-dimensional natural frequency

Fig. 8 Variations of first two natural frequencies of a simply supported FG nanoplate with respect to power-law index k and even type of porosity coefficients ξ and various amounts of elastic Kerr foundation parameters.

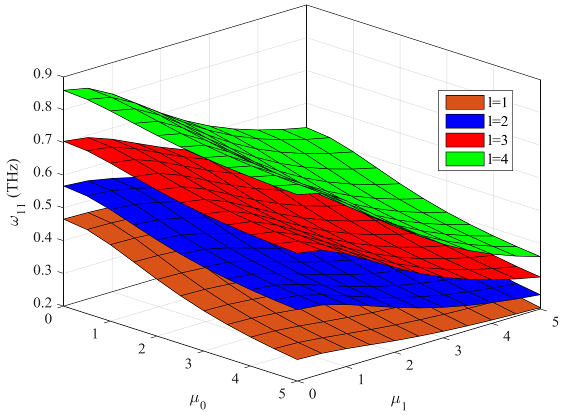

(a) First non-dimensional natural frequency

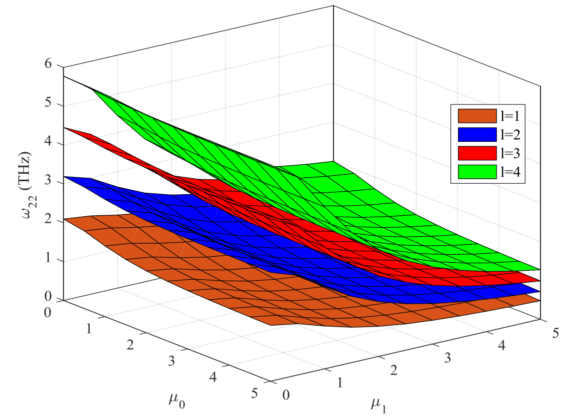

(b) Second non-dimensional natural frequency

Fig. 9 Variations of first two natural frequencies of a simply supported FG nanoplate with nonlocal parameters and different values of strain gradient length scale.

FG nanoplate are summarized in Table 9. Results are obtained when (k=1, $\mu_0=\mu_1$=2nm, l=1nm). Also, the results have shown the effects of different geometrical parameters (i.e. aspect ratio (varying from 1 to 2), length-to-thickness ratio (varying from 2 to 50). According to the high accuracy of the present model, the results can be as a benchmark for future works on the vibration analysis of perfect and imperfect FG nanosize plates.

Next, the effect of elastic Kerr foundation parameters on the first non-dimensional natural frequency of the FG nanoplate under three different types of porosity is analyzed. So, the obtained results for three cases (i.e. classical (scaling free), nonlocal strain gradient elasticity theory ($\mu_0=\mu_1=\mu$) and higher-order nonlocal strain gradient elasticity theory) are listed in Table 10, which it can be considered as the benchmark results for further comparisons. Then, to better illustrate the impact of foundation parameters, the variations of first two natural frequencies of porous FG nanosize plate on elastic substrate with respect to material compositions (power-law indices k) and even type of porosities for different Kerr foundation parameters is plotted in Fig. 8 when (a/h=10, b/a=, $\mu_0=\mu_1$=2nm, l=1nm). To simplify the issue, it is assumed that stiffness of upper and lower springs of Kerr foundation are identical. We can see that the stiffness of springs increases, the natural frequency increases as well. In fact, the FG nanoplate becomes more rigid with an increase in springs stiffness leading. Also, it may be concluded that the presence of shear layer of foundation provides a continuous interaction with the nanoplate and raises the natural frequency. Therefore, the Kerr foundation may cause to an increase in natural frequencies of FG nanoplates, as it has been discussed in several other researches in the literature. In addition, it is seen that the linear layer parameters have less influences on the frequencies in comparison with the shear layer of this foundation.

As final study, effects of increasing higher/-lower order nonlocal parameters on the variations of first-two natural frequencies of mounted imperfect FG nanoplates in hygrothermal environment are studied in Fig. 9. Results are plotted for different values of strain gradient length scale when a/h=10, b/a=1, k=1, ξ=0.2, ΔT=50, ΔH=0.5, $K_l=K_u$=20, K_s=10. As we expected, increasing the nonlocal parameters is one of the main reasons of decreasing the natural frequencies of imperfect FG nanosize plates here.

Additionally, variations in nonlocal length scale parameter will cause more influences on higher-order frequencies. Besides, no matter how much the gradient length scale rises, the higher-order nonlocal parameter will force more influences on the natural frequencies of imperfect FG nanosize plates compared with the nonlocal parameter of lower-order.

5. Conclusions

In this paper, hygrothermal vibration response of size-dependent functionally graded nanoplates containing porosities were studied using an analytical method. The FG porous nanoplate was rested on a three-parametric elastic foundation which includes the upper/lower spring layers and a shear layer, namely Kerr foundation. Material properties were represented via a modified power-law distribution, while the governing equations were obtained through the principles of Hamilton and virtual work based on the second shear deformation theory of plates in conjunction with the higher-order nonlocal strain gradient elasticity theory. Then, the Navier solution method was used to solve the equations of motion of the FG nanoplate for simply supported boundary conditions. Afterwards, numerical results were presented to study the effects of material composition, three different types of porosity, small scale parameters, moisture and temperature differences and elastic Kerr foundation parameters. Based on a wide parametric investigation, the essential conclusions can be summarized as follows:

- An increase in the power-law indices can causes to a large amount of decrease in the natural frequency.
- Rising the natural frequency could be inflected by rising (decreasing) the strain gradient length scale (nonlocal parameter).
- As far as mode of frequency is concerned, the higher-order frequencies are more under influence of small-scale parameters compared with lower-order frequencies.
- Raising the moisture and temperature differences reduce the natural frequency of the FG nanoplate considerably so that it is mandatory to obtain their results for an accurate analysis on porous materials.
- The elastic Kerr foundation can be selected as a powerful parameter to the aim of rising the natural frequencies of FG nanoplates.

References

Aghababaei, R. and Reddy, J. (2009), "Nonlocal third-order shear deformation plate theory with application to bending and vibration of plates", *J. Sound Vib.*, **326**(1), 277-289. https://doi.org/10.1016/j.jsv.2009.04.044.

Andrews, E., Gioux, G., Onck, P. and Gibson, L. (2001), "Size effects in ductile cellular solids. Part II: experimental results", *J. Mech. Sci.*, **43**(3), 701-713. https://doi.org/10.1016/S0020-7403(00)00043-6.

Askes, H. and Aifantis, E.C. (2011), "Gradient elasticity in statics and dynamics: an overview of formulations, length scale identification procedures, finite element implementations and new results", *J. Solids Struct.*, **48**(13), 1962-1990. https://doi.org/10.1016/j.ijsolstr.2011.03.006.

Atmane, H.A., Tounsi, A. and Bernard, F. (2017), "Effect of thickness stretching and porosity on mechanical response of a functionally graded beams resting on elastic foundations", *J. Mech. Mater. Design*, **13**(1), 71-84. https://doi.org/10.1007/s10999-015-9318-x.

Barati, M.R. (2017), "On wave propagation in nanoporous materials", *J. Eng. Sci.*, **116**, 1-11. https://doi.org/10.1016/j.ijengsci.2017.03.007.

Barati, M.R. and Zenkour, A. (2017), "A general bi-Helmholtz nonlocal strain-gradient elasticity for wave propagation in nanoporous graded double-nanobeam systems on elastic substrate", *Compos. Struct.*, **168**, 885-892. https://doi.org/10.1016/j.compstruct.2017.02.090.

Duan, W., Wang, C. and Zhang, Y. (2007), "Calibration of nonlocal scaling effect parameter for free vibration of carbon nanotubes by molecular dynamics", *J. Appl. Phys.*, **101**(2), 024305. https://doi.org/10.1063/1.2423140.

Ebrahimi, F. and Barati, M.R. (2018), "Wave propagation analysis of smart strain gradient piezo-magneto-elastic nonlocal beams", *Struct. Eng. Mech.*, **66**(2), 237-248. https://doi.org/10.12989/sem.2018.66.2.237.

Eringen, A.C. and Edelen, D. (1972), "On nonlocal elasticity", *J. Eng. Sci.*, **10**(3), 233-248. https://doi.org/10.1016/0020-7225(72)90039-0.

Farzam-Rad, S.A., Hassani, B. and Karamodin, A. (2017), "Isogeometric analysis of functionally graded plates using a new quasi-3D shear deformation theory based on physical neutral surface", *Compos. Part B Eng.*, **108**, 174-189. https://doi.org/10.1016/j.compositesb.2016.09.029.

Ghayesh, M.H. (2018), "Functionally graded microbeams: simultaneous presence of imperfection and viscoelasticity", *IJ. Mech. Sci.*, **140**, 339-350. https://doi.org/10.1016/j.ijmecsci.2018.02.037.

Ghayesh, M.H. (2018), "Nonlinear vibration analysis of axially functionally graded shear-deformable tapered beams", *Applied Mathematical Modelling*. **59**, 583-596. https://doi.org/10.1016/j.apm.2018.02.017.

Ghayesh, M.H. (2019), "Viscoelastic dynamics of axially FG microbeams", *J. Eng. Sci.*, **135**, 75-85. https://doi.org/10.1016/j.ijengsci.2018.10.005.

Ghayesh, M.H., Amabili, M. and Farokhi, H. (2013), "Three-dimensional nonlinear size-dependent behaviour of Timoshenko microbeams", *J. Eng. Sci.*, **71**, 1-14. https://doi.org/10.1016/j.ijengsci.2013.04.003.

Ghayesh, M.H., Farokhi, H. and Alici, G. (2016), "Size-dependent performance of microgyroscopes", *J. Eng. Sci.*, **100**, 99-111. https://doi.org/10.1016/j.ijengsci.2015.11.003.

Gholipour, A., Farokhi, H. and Ghayesh, M.H. (2015), "In-plane and out-of-plane nonlinear size-dependent dynamics of microplates", *Nonlinear Dynam.*, **79**(3), 1771-1785. https://doi.org/10.1007/s11071-014-1773-7.

Jin, G., Su, Z., Shi, S., Ye, T. and Gao, S. (2014), "Three-dimensional exact solution for the free vibration of arbitrarily thick functionally graded rectangular plates with general boundary conditions", *Compos. Struct.*, **108**, 565-577. https://doi.org/10.1016/j.compstruct.2013.09.051.

Kar, V.R., Mahapatra, T.R. and Panda, S.K. (2015), "Nonlinear flexural analysis of laminated composite flat panel under hygro-thermo-mechanical loading", *Steel Compos. Struct.*, **19**(4), 1011-1033. https://doi.org/10.1142/S0219876216500158.

Karami, B., Janghorban, M. and Rabczuk, T. (2019), "Analysis of elastic bulk waves in functionally graded triclinic nanoplates using a quasi-3D bi-Helmholtz nonlocal strain gradient model", *European J. Mech. A/Solids*. **78**, 103822. https://doi.org/10.1016/j.euromechsol.2019.103822.

Karami, B., Janghorban, M., Shahsavari, D. and Tounsi, A. (2018), "A size-dependent quasi-3D model for wave dispersion analysis of FG nanoplates", *Steel Compos. Struct.*, **28**(1), 99-110. https://doi.org/10.12989/scs.2018.28.1.099.

Karami, B., Janghorban, M. and Tounsi, A. (2017), "Effects of triaxial magnetic field on the anisotropic nanoplates", *Steel and Compos. Struct.*, **25**(3), 361-374. https://doi.org/10.12989/scs.2017.25.3.361.

Karami, B., Janghorban, M. and Tounsi, A. (2018), "Variational approach for wave dispersion in anisotropic doubly-curved nanoshells based on a new nonlocal strain gradient higher order shell theory", *Thin Wall Struct.*, **129**, 251-264. https://doi.org/10.1016/j.tws.2018.02.025.

Karami, B., janghorban, M. and Tounsi, A. (2019), "On exact wave propagation analysis of triclinic material using three-dimensional bi-Helmholtz gradient plate model", *Struct. Eng. Mech.*, **69**(5), 487-497. https://doi.org/10.12989/sem.2019.69.5.487.

Karami, B., Shahsavari, D. and Janghorban, M. (2018), "A comprehensive analytical study on functionally graded carbon nanotube-reinforced composite plates", *Aerosp. Sci. Technol.*, **82**, 499-512. https://doi.org/10.1016/j.ast.2018.10.001.

Karami, B., Shahsavari, D., Janghorban, M. and Li, L. (2018), "Wave dispersion of mounted graphene with initial stress", *Thin Wall Struct.*, **122**, 102-111. https://doi.org/10.1016/j.tws.2017.10.004.

Karami, B., Shahsavari, D., Janghorban, M. and Li, L. (2019), "On the resonance of functionally graded nanoplates using bi-Helmholtz nonlocal strain gradient theory", *J. Eng. Sci.*, **144**, 103143. https://doi.org/10.1016/j.ijengsci.2019.103143.

Karami, B., Shahsavari, D. and Li, L. (2018), "Hygrothermal wave propagation in viscoelastic graphene under in-plane magnetic field based on nonlocal strain gradient theory", *Physica E Low-dimensional Syst. Nanostruct.*, **97**, 317-327. https://doi.org/10.1016/j.physe.2017.11.020.

Karami, B., Shahsavari, D. and Li, L. (2018), "Temperature-dependent flexural wave propagation in nanoplate-type porous heterogenous material subjected to in-plane magnetic field", *J. Thermal Stress.*, **41**(4), 483-499. https://doi.org/10.1080/01495739.2017.1393781.

Karami, B., Shahsavari, D., Li, L., Karami, M. and Janghorban, M. (2019), "Thermal buckling of embedded sandwich piezoelectric nanoplates with functionally graded core by a nonlocal second-order shear deformation theory", *Proc. Institution of Mech. Eng., Part C J. Mech. Eng. Sci.*, **233**(1), 287-301. https://doi.org/10.1177/0954406218756451.

Khdeir, A. and Reddy, J. (1999), "Free vibrations of laminated composite plates using second-order shear deformation theory", *Comput. Struct.*, **71**(6), 617-626. https://doi.org/10.1016/S0045-7949(98)00301-0.

Kneifati, M.C. (1985), "Analysis of plates on a Kerr foundation model", *J. Eng. Mech.*, **111**(11), 1325-1342. https://doi.org/10.1061/(ASCE)0733-9399(1985)111:11(1325).

Koh, S. and Lee, H. (2006), "Molecular dynamics simulation of size and strain rate dependent mechanical response of FCC metallic nanowires", *Nanotechnology*, **17**(14), 3451. https://doi.org/10.1088/0957-4484/17/14/018.

Lam, D.C., Yang, F., Chong, A., Wang, J. and Tong, P. (2003), "Experiments and theory in strain gradient elasticity", *J. Mech. Phys. Solids*, **51**(8), 1477-1508. https://doi.org/10.1016/S0022-5096(03)00053-X.

Li, L. and Hu, Y. (2016), "Nonlinear bending and free vibration analyses of nonlocal strain gradient beams made of functionally graded material", *J. Eng. Sci.*, **107**, 77-97. https://doi.org/10.1016/j.ijengsci.2016.07.011.

Li, L. and Hu, Y. (2017), "Post-buckling analysis of functionally graded nanobeams incorporating nonlocal stress and microstructure-dependent strain gradient effects", *IJ. Mech. Sci.*, **120**, 159-170. https://doi.org/10.1016/j.ijmecsci.2016.11.025.

Li, L., Hu, Y. and Ling, L. (2015), "Flexural wave propagation in small-scaled functionally graded beams via a nonlocal strain gradient theory", *Compos. Struct.*, **133**, 1079-1092. https://doi.org/10.1016/j.compstruct.2015.08.014.

Lim, C., Zhang, G. and Reddy, J. (2015), "A higher-order nonlocal elasticity and strain gradient theory and its applications in wave propagation", *J. Mech. Phys. Solids* **78**, 298-313. https://doi.org/10.1016/j.jmps.2015.02.001.

Magnucki, K., Malinowski, M. and Kasprzak, J. (2006), "Bending and buckling of a rectangular porous plate", *Steel and Compos. Struct.*, **6**(4), 319-333. https://doi.org/10.12989/scs.2006.6.4.319.

Mahapatra, T., Kar, V. and Panda, S. (2016), "Large amplitude vibration analysis of laminated composite spherical panels under hygrothermal environment", *J. Struct. Stability Dynam.*, **16**(03), 1450105. https://doi.org/10.1142/S0219455414501053.

Mahapatra, T., Panda, S. and Kar, V. (2016), "Geometrically nonlinear flexural analysis of hygro-thermo-elastic laminated composite doubly curved shell panel", *J. Mech. Mater. Design*, **12**(2), 153-171. https://doi.org/10.1007/s10999-015-9299-9.

Mahapatra, T., Panda, S.K. and Kar, V.R. (2016), "Nonlinear hygro-thermo-elastic vibration analysis of doubly curved composite shell panel using finite element micromechanical model", *Mech. Adv. Mater. Struct.*, **23**(11), 1343-1359. https://doi.org/10.1080/15376494.2015.1085606.

Mahapatra, T.R., Kar, V.R., Panda, S.K. and Mehar, K. (2017), "Nonlinear thermoelastic deflection of temperature-dependent FGM curved shallow shell under nonlinear thermal loading", *J. Thermal Stress.*, **40**(9), 1184-1199. https://doi.org/10.1080/01495739.2017.1302788.

Mechab, I., Mechab, B., Benaissa, S., Serier, B. and Bouiadjra, B.B. (2016), "Free vibration analysis of FGM nanoplate with porosities resting on Winkler Pasternak elastic foundations based on two-variable refined plate theories", *J. Brazilian Soc. Mech. Sci. Eng.*, **38**(8), 2193-2211. https://doi.org/10.1007/s40430-015-0482-6.

Mehar, K. and Panda, S.K. (2016), "Nonlinear static behavior of FG-CNT reinforced composite flat panel under thermomechanical load", *J. Aerosp. Eng.*, **30**(3), 04016100. https://doi.org/10.1061/(ASCE)AS.1943-5525.0000706.

Mehar, K. and Panda, S.K. (2017), "Numerical investigation of nonlinear thermomechanical deflection of functionally graded CNT reinforced doubly curved composite shell panel under different mechanical loads", *Compos. Struct.*, **161**, 287-298. https://doi.org/10.1016/j.compstruct.2016.10.135.

Mehar, K., Panda, S.K., Bui, T.Q. and Mahapatra, T.R. (2017), "Nonlinear thermoelastic frequency analysis of functionally graded CNT-reinforced single/doubly curved shallow shell panels by FEM", *J. Thermal Stress.*, **40**(7), 899-916. https://doi.org/10.1080/01495739.2017.1318689.

Mehar, K., Panda, S.K. and Mahapatra, T.R. (2017), "Theoretical and experimental investigation of vibration characteristic of carbon nanotube reinforced polymer composite structure", *IJ. Mech. Sci.*. **133**, 319-329. https://doi.org/10.1016/j.ijmecsci.2017.08.057.

Mehar, K., Panda, S.K. and Mahapatra, T.R. (2017), "Thermoelastic nonlinear frequency analysis of CNT reinforced functionally graded sandwich structure", *European. J. Mech. A/Solids.*, **65**, 384-396. https://doi.org/10.1016/j.euromechsol.2017.05.005.

Mehar, K., Panda, S.K. and Patle, B.K. (2017), "Thermoelastic vibration and flexural behavior of FG-CNT reinforced composite curved panel", *J. Appl. Mech.*, **9**(04), 1750046. https://doi.org/10.1142/S1758825117500466.

Miyamoto, Y., Kaysser, W., Rabin, B., Kawasaki, A. and Ford, R.G. (2013), *Functionally graded materials: design, processing and applications*, Springer Science & Business Medi, Germany.

Mohammadi, H. and Mahzoon, M. (2014), "Investigating thermal effects in nonlinear buckling analysis of micro beams using modified strain gradient theory", *Iran. J. Sci. Technol. Transaction. Mech. Eng.*, **38**(M2), 303.

Mohammadi, H., Mahzoon, M., Mohammadi, M. and Mohammadi, M. (2014), "Postbuckling instability of nonlinear nanobeam with geometric imperfection embedded in elastic foundation", *Nonlinear Dynam.*, **76**(4), 2005-2016. https://doi.org/10.1007/s11071-014-1264-x.

Mousavi, S.M. (2016), "Dislocation-based fracture mechanics within nonlocal and gradient elasticity of bi-Helmholtz type–Part I: Antiplane analysis", *J. Solids Struct.*, **87**, 222-235. https://doi.org/10.1016/j.ijsolstr.2015.10.033.

Nematollahi, M.S., Mohammadi, H. and Nematollahi, M.A. (2017), "Thermal vibration analysis of nanoplates based on the higher-order nonlocal strain gradient theory by an analytical approach", *Superlattices Microstruct.*, **111**, 944-959. https://doi.org/10.1016/j.spmi.2017.07.055.

Rad, A.B. and Shariyat, M. (2015), "Three-dimensional magneto-elastic analysis of asymmetric variable thickness porous FGM circular plates with non-uniform tractions and Kerr elastic foundations", *Compos. Struct.*, **125**, 558-574. https://doi.org/10.1016/j.compstruct.2015.02.049.

Romano, G., Barretta, R., Diaco, M. and de Sciarra, F.M. (2017), "Constitutive boundary conditions and paradoxes in nonlocal elastic nanobeams", *IJ. Mech. Sci.*, **121**, 151-156. https://doi.org/10.1016/j.ijmecsci.2016.10.036.

Shafiei, N., Mousavi, A. and Ghadiri, M. (2016), "On size-dependent nonlinear vibration of porous and imperfect functionally graded tapered microbeams", *J. Eng. Sci.*, **106**, 42-56. https://doi.org/10.1016/j.ijengsci.2016.05.007.

Shahsavari, D., Shahsavari, M., Li, L. and Karami, B. (2018), "A novel quasi-3D hyperbolic theory for free vibration of FG plates with porosities resting on Winkler/Pasternak/Kerr foundation", *Aerosp. Sci. Technol.*, **72**, 134-149. https://doi.org/10.1016/j.ast.2017.11.004.

Shahverdi, H. and Barati, M.R. (2017), "Vibration analysis of porous functionally graded nanoplates", *J. Eng. Sci.*, **120** 82-99. https://doi.org/10.1016/j.ijengsci.2017.06.008.

Shen, L., Shen, H.-S. and Zhang, C.-L. (2010), "Nonlocal plate model for nonlinear vibration of single layer graphene sheets in thermal environments", *Comput. Mater. Sci.*, **48**(3), 680-685. https://doi.org/10.1016/j.commatsci.2010.03.006.

Şimşek, M. and Aydın, M. (2017), "Size-dependent forced vibration of an imperfect functionally graded (FG) microplate with porosities subjected to a moving load using the modified couple stress theory", *Compos. Struct.*, **160**, 408-421. https://doi.org/10.1016/j.compstruct.2016.10.034.

Thai, H.-T., Vo, T.P., Nguyen, T.-K. and Kim, S.-E. (2017), "A review of continuum mechanics models for size-dependent analysis of beams and plates", *Compos. Struct.*, **177**, 196-219. https://doi.org/10.1016/j.compstruct.2017.06.040.

Wattanasakulpong, N. and Ungbhakorn, V. (2014), "Linear and nonlinear vibration analysis of elastically restrained ends FGM beams with porosities", *Aerosp. Sci. Technol.*, **32**(1), 111-120. https://doi.org/10.1016/j.ast.2013.12.002.

Xiao, W., Li, L. and Wang, M. (2017), "Propagation of in-plane wave in viscoelastic monolayer graphene via nonlocal strain gradient theory", *Appl. Physics A.*, **123**(6), 388. https://doi.org/10.1007/s00339-017-1007-1.

Yahia, S.A., Atmane, H.A., Houari, M.S.A. and Tounsi, A. (2015), "Wave propagation in functionally graded plates with porosities using various higher-order shear deformation plate theories", *Struct. Eng. Mech.*, **53**(6), 1143-1165. https://doi.org/10.12989/sem.2015.53.6.1143.

Zemri, A., Houari, M.S.A., Bousahla, A.A. and Tounsi, A. (2015), "A mechanical response of functionally graded nanoscale beam: an assessment of a refined nonlocal shear deformation theory beam theory", *Struct. Eng. Mech.*, **54**(4), 693-710. https://doi.org/10.12989/sem.2015.54.4.693.

Zhao, J., Choe, K., Xie, F., Wang, A., Shuai, C. and Wang, Q. (2018), "Three-dimensional exact solution for vibration analysis of thick functionally graded porous (FGP) rectangular plates with arbitrary boundary conditions", *Compos. Part B Eng.*, **155**, 369-381. https://doi.org/10.1016/j.compositesb.2018.09.001.

CC

Appendix

$$\mathcal{L}_l\left(A_{11}\frac{\partial^2 u}{\partial x^2}+A_{66}\frac{\partial^2 u}{\partial y^2}+A_{12}\frac{\partial^2 v}{\partial x\,\partial y}+A_{66}\frac{\partial^2 v}{\partial x\,\partial y}+B_{11}\frac{\partial^2 \varphi_1}{\partial x^2}\right)$$
$$+\mathcal{L}_l\left(B_{66}\frac{\partial^2 \varphi_1}{\partial y^2}+D_{11}\frac{\partial^2 \varphi_2}{\partial x^2}D_{66}\frac{\partial^2 \varphi_2}{\partial y^2}+B_{12}\frac{\partial^2 \psi_1}{\partial x\,\partial y}+B_{66}\frac{\partial^2 \psi_1}{\partial x\,\partial y}\right) \tag{1}$$
$$+\mathcal{L}_l\left(+D_{12}\frac{\partial^2 \psi_2}{\partial x\,\partial y}+D_{66}\frac{\partial^2 \psi_2}{\partial x\,\partial y}\right)=\mathcal{L}_\mu\left(I_0\frac{\partial^2 u}{\partial t^2}+I_1\frac{\partial^2 \varphi_1}{\partial t^2}+I_2\frac{\partial^2 \varphi_2}{\partial t^2}\right)$$

$$\mathcal{L}_l\left(A_{12}\frac{\partial^2 u}{\partial x\,\partial y}+A_{66}\frac{\partial^2 u}{\partial x\,\partial y}+A_{22}\frac{\partial^2 v}{\partial y^2}+A_{66}\frac{\partial^2 v}{\partial x^2}+B_{12}\frac{\partial^2 \varphi_1}{\partial x\,\partial y}\right)$$
$$+\mathcal{L}_l\left(+B_{66}\frac{\partial^2 \varphi_1}{\partial x\,\partial y}+D_{12}\frac{\partial^2 \varphi_2}{\partial x\,\partial y}+D_{66}\frac{\partial^2 \varphi_2}{\partial x\,\partial y}+B_{22}\frac{\partial^2 \psi_1}{\partial y^2}+B_{66}\frac{\partial^2 \psi_1}{\partial x^2}\right) \tag{2}$$
$$+\mathcal{L}_l\left(D_{22}\frac{\partial^2 \psi_2}{\partial y^2}+D_{66}\frac{\partial^2 \psi_2}{\partial x^2}\right)=\mathcal{L}_\mu\left(I_0\frac{\partial^2 v}{\partial t^2}+I_1\frac{\partial^2 \psi_1}{\partial t^2}+I_2\frac{\partial^2 \psi_2}{\partial t^2}\right)$$

$$\mathcal{L}_l\left(A_{44}\frac{\partial^2 w}{\partial y^2}+A_{55}\frac{\partial^2 w}{\partial x^2}+A_{55}\frac{\partial \varphi_1}{\partial x}+2B_{55}\frac{\partial \varphi_2}{\partial x}\right)$$
$$+\mathcal{L}_l\left(+A_{44}\frac{\partial \psi_1}{\partial y}+2B_{44}\frac{\partial \psi_2}{\partial y}\right)=\mathcal{L}_\mu\left(I_0\frac{\partial^2 w}{\partial t^2}+\left(\frac{k_l k_u}{k_l+k_u}\right)w\right) \tag{3}$$
$$+\mathcal{L}_\mu\left((N^T+N^H-\frac{k_s k_u}{k_l+k_u})(\frac{\partial^2 w}{\partial x^2}+\frac{\partial^2 w}{\partial y^2})\right)$$

$$\mathcal{L}_l\left(B_{11}\frac{\partial^2 u}{\partial x^2}+B_{66}\frac{\partial^2 u}{\partial y^2}+B_{12}\frac{\partial^2 v}{\partial x\,\partial y}+B_{66}\frac{\partial^2 v}{\partial x\,\partial y}-A_{55}\frac{\partial w}{\partial x}\right)$$
$$+\mathcal{L}_l\left(+D_{11}\frac{\partial^2 \varphi_1}{\partial x^2}+D_{66}\frac{\partial^2 \varphi_1}{\partial y^2}-A_{55}\varphi_1+E_{11}\frac{\partial^2 \varphi_2}{\partial x^2}+E_{66}\frac{\partial^2 \varphi_2}{\partial y^2}\right)$$
$$+\mathcal{L}_l\left(-2B_{55}\varphi_2+D_{12}\frac{\partial^2 \psi_1}{\partial x\,\partial y}+D_{66}\frac{\partial^2 \psi_1}{\partial x\,\partial y}+E_{12}\frac{\partial^2 \psi_2}{\partial x\,\partial y}+E_{66}\frac{\partial^2 \psi_2}{\partial x\,\partial y}\right) \tag{4}$$
$$=\mathcal{L}_\mu\left(I_1\frac{\partial^2 u}{\partial t^2}+I_2\frac{\partial^2 \varphi_1}{\partial t^2}+I_3\frac{\partial^2 \varphi_2}{\partial t^2}\right)$$

$$\mathcal{L}_l\left(D_{11}\frac{\partial^2 u}{\partial x^2}+D_{66}\frac{\partial^2 u}{\partial y^2}+D_{12}\frac{\partial^2 v}{\partial x\,\partial y}+D_{66}\frac{\partial^2 v}{\partial x\,\partial y}-2B_{55}\frac{\partial w}{\partial x}\right)$$
$$+\mathcal{L}_l\left(E_{11}\frac{\partial^2 \varphi_1}{\partial x^2}+E_{66}\frac{\partial^2 \varphi_1}{\partial y^2}-2B_{55}\varphi_1+F_{11}\frac{\partial^2 \varphi_2}{\partial x^2}+F_{66}\frac{\partial^2 \varphi_2}{\partial y^2}\right)$$
$$+\mathcal{L}_l\left(-4D_{55}\varphi_2+E_{12}\frac{\partial^2 \psi_1}{\partial x\,\partial y}+E_{66}\frac{\partial^2 \psi_1}{\partial x\,\partial y}+F_{12}\frac{\partial^2 \psi_2}{\partial x\,\partial y}+F_{66}\frac{\partial^2 \psi_2}{\partial x\,\partial y}\right) \tag{5}$$
$$=\mathcal{L}_\mu\left(I_2\frac{\partial^2 u}{\partial t^2}+I_3\frac{\partial^2 \varphi_1}{\partial t^2}+I_4\frac{\partial^2 \varphi_2}{\partial t^2}\right)$$

$$\mathcal{L}_l\left(B_{12}\frac{\partial^2 u}{\partial x\partial y}+B_{66}\frac{\partial^2 u}{\partial x\partial y}+B_{22}\frac{\partial^2 v}{\partial y^2}+B_{66}\frac{\partial^2 v}{\partial x^2}-A_{44}\frac{\partial w}{\partial y}\right)$$
$$+\mathcal{L}_l\left(+D_{12}\frac{\partial^2 \varphi_1}{\partial x\partial y}+D_{66}\frac{\partial^2 \varphi_1}{\partial x\partial y}+E_{12}\frac{\partial^2 \varphi_2}{\partial x\partial y}+E_{66}\frac{\partial^2 \varphi_2}{\partial x\partial y}-2B_{55}\varphi_2\right) \tag{6}$$
$$+\mathcal{L}_l\left(D_{22}\frac{\partial^2 \psi_1}{\partial y^2}+D_{66}\frac{\partial^2 \psi_1}{\partial x^2}-A_{44}\psi_1E_{22}\frac{\partial^2 \psi_2}{\partial y^2}+E_{66}\frac{\partial^2 \psi_2}{\partial x^2}-2B_{44}\psi_2\right)$$
$$=\mathcal{L}_\mu\left(I_1\frac{\partial^2 v}{\partial t^2}+I_2\frac{\partial^2 \psi_1}{\partial t^2}+I_3\frac{\partial^2 \psi_2}{\partial t^2}\right)$$

$$\mathcal{L}_l\left(D_{12}\frac{\partial^2 u}{\partial x\,\partial y}+D_{66}\frac{\partial^2 u}{\partial x\,\partial y}+D_{22}\frac{\partial^2 v}{\partial y^2}+D_{66}\frac{\partial^2 v}{\partial x^2}-2B_{44}\frac{\partial w}{\partial y}\right)$$
$$+\mathcal{L}_l\left(E_{12}\frac{\partial^2 \varphi_1}{\partial x\,\partial y}+E_{66}\frac{\partial^2 \varphi_1}{\partial x\,\partial y}+F_{12}\frac{\partial^2 \varphi_2}{\partial x\,\partial y}+F_{66}\frac{\partial^2 \varphi_2}{\partial x\,\partial y}+E_{22}\frac{\partial^2 \psi_1}{\partial y^2}\right)$$
$$+\mathcal{L}_l\left(E_{66}\frac{\partial^2 \psi_1}{\partial x^2}-2B_{44}\psi_1F_{22}\frac{\partial^2 \psi_2}{\partial y^2}+F_{66}\frac{\partial^2 \psi_2}{\partial x^2}-4D_{44}\psi_2\right) \tag{7}$$
$$=\mathcal{L}_\mu\left(I_2\frac{\partial^2 v}{\partial t^2}+I_3\frac{\partial^2 \psi_1}{\partial t^2}+I_4\frac{\partial^2 \psi_2}{\partial t^2}\right)$$

Table 8 First non-dimensional frequency of FG nanoplate affected by different porosity pattern (μ_0=μ_1=2nm, l=1nm)

b/a	a/h	Perfect (ξ=0)			Even porosity (ξ=0.2)			Uneven porosity (ξ=0.2)			Logarithmic-uneven porosity (ξ=0.2)		
		k=0.2	k=1	k=5	k=0.2	k=1	k=5	k=0.2	k=1	k=5	k=0.2	k=1	k=5
1	2	1.45901	1.21681	0.98566	1.49142	1.17073	0.78114	1.48601	1.21639	0.92879	1.48466	1.21648	0.93230
	5	0.32069	0.26457	0.22316	0.32728	0.25140	0.17551	0.32867	0.26629	0.21510	0.32827	0.26622	0.21562
	10	0.08652	0.07122	0.06010	0.08825	0.06744	0.04806	0.08889	0.07189	0.05938	0.08877	0.07186	0.05949
	20	0.02211	0.01818	0.01565	0.02254	0.01720	0.01235	0.02273	0.01838	0.01529	0.02270	0.01837	0.01532
	50	0.00356	0.00293	0.00252	0.00363	0.00277	0.00199	0.00366	0.00296	0.00247	0.00366	0.00296	0.00247
2	2	1.08275	0.89936	0.73684	1.10624	0.86169	0.58119	1.10469	0.90056	0.69831	1.10359	0.90055	0.70071
	5	0.22033	0.18158	0.15421	0.22480	0.17227	0.12135	0.22606	0.18300	0.14929	0.22577	0.18294	0.14961
	10	0.05795	0.04769	0.04094	0.05911	0.04514	0.03227	0.05956	0.04816	0.03992	0.05947	0.04814	0.03999
	20	0.01469	0.01208	0.01041	0.01498	0.01143	0.00821	0.01511	0.01221	0.01017	0.01508	0.01221	0.01019
	50	0.00236	0.00194	0.00167	0.00241	0.00184	0.00132	0.00243	0.00196	0.00164	0.00242	0.00196	0.00164

Table 9 First three non-dimensional frequencies of S-S rectangular FG nanoplate affected by different porosity patterns (k=1, μ_0=μ_1=2nm, l=1nm)

b/a	a/h	Perfect (ξ=0)			Even porosity (ξ=0.2)			Uneven porosity (ξ=0.2)			Logarithmic-uneven porosity (ξ=0.2)		
		$\tilde{\omega}_{11}$	$\tilde{\omega}_{22}$	$\tilde{\omega}_{33}$	$\tilde{\omega}_{11}$	$\tilde{\omega}_{22}$	$\tilde{\omega}_{33}$	$\tilde{\omega}_{11}$	$\tilde{\omega}_{22}$	$\tilde{\omega}_{33}$	$\tilde{\omega}_{11}$	$\tilde{\omega}_{22}$	$\tilde{\omega}_{33}$
1	2	1.21681	2.50478	3.34691	1.17073	2.44536	3.00339	1.21639	2.49797	3.25648	1.21648	2.49842	3.26110
	5	0.26457	0.69316	1.13453	0.25140	0.66425	1.09553	0.26629	0.69401	1.13296	0.26622	0.69401	1.13310
	10	0.07122	0.21219	0.38635	0.06744	0.20163	0.36867	0.07189	0.21357	0.38772	0.07186	0.21351	0.38767
	20	0.01818	0.05711	0.11096	0.01720	0.05409	0.10524	0.01838	0.05766	0.11186	0.01837	0.05763	0.11182
	50	0.00293	0.00936	0.01868	0.00277	0.00885	0.01767	0.00296	0.00946	0.01887	0.00296	0.00945	0.01886
2	2	0.89936	2.00261	2.92806	0.86169	1.94516	2.67432	0.90056	1.99781	2.85764	0.90055	1.99815	2.86151
	5	0.18158	0.51112	0.85608	0.17227	0.48807	0.82284	0.18300	0.51271	0.85608	0.18294	0.51266	0.85612
	10	0.04769	0.14837	0.27364	0.04514	0.14076	0.26042	0.04816	0.14953	0.27511	0.04814	0.14948	0.27505
	20	0.01208	0.03896	0.07542	0.01143	0.03688	0.07145	0.01221	0.03935	0.07610	0.01221	0.03934	0.07607
	50	0.00194	0.00633	0.01247	0.00184	0.00597	0.01180	0.00196	0.00640	0.01260	0.00196	0.00639	0.01259

Table 10 First non-dimensional frequency of FG nanoplate affected by different porosity patterns versus elastic Kerr foundation, (a/h=20, k=1)

	K_s	K_l=K_u	Perfect	Even		Uneven		Logarithmic-uneven	
			ξ=0	ξ=0.1	ξ=0.2	ξ=0.1	ξ=0.2	ξ=0.1	ξ=0.2
μ_0=μ_1=l=0	5	10	0.02280	0.02239	0.02178	0.02295	0.02309	0.02294	0.02308
		20	0.02285	0.02245	0.02185	0.02300	0.02315	0.02300	0.02314
		30	0.02291	0.02250	0.02192	0.02305	0.02321	0.02304	0.02319
	10	10	0.02331	0.02296	0.02244	0.02348	0.02365	0.02347	0.02363
		20	0.02336	0.02302	0.02251	0.02353	0.02370	0.02352	0.23069
		30	0.02341	0.02307	0.02257	0.02358	0.02376	0.02358	0.02374
μ_0=μ_1=μ=1, l=2	5	10	0.02765	0.02711	0.02633	0.02781	0.02798	0.02781	0.02796
		20	0.02769	0.02716	0.02638	0.02786	0.02802	0.02785	0.02801
		30	0.02773	0.02721	0.02644	0.02790	0.02807	0.02790	0.02806
	10	10	0.02807	0.02758	0.02688	0.02825	0.02844	0.02825	0.02842
		20	0.02811	0.02763	0.02693	0.02830	0.02849	0.02829	0.02847
		30	0.02815	0.02768	0.02699	0.02834	0.02853	0.02833	0.02851
μ_0=4, μ_1=1, l=2	5	10	0.02169	0.02130	0.02074	0.02183	0.02197	0.02183	0.02196
		20	0.02174	0.02137	0.02081	0.02189	0.02203	0.02188	0.02202
		30	0.02180	0.02143	0.02088	0.02194	0.02209	0.02194	0.02208
	10	10	0.02222	0.02190	0.02143	0.02239	0.02255	0.02238	0.02254
		20	0.02228	0.02196	0.02150	0.02244	0.02261	0.02244	0.02260
		30	0.02233	0.02202	0.02157	0.02250	0.02267	0.02249	0.02265
μ_0=1, μ_1=4, l=2	5	10	0.02307	0.02265	0.02203	0.02322	0.02336	0.02321	0.02335
		20	0.02312	0.02271	0.02210	0.02327	0.02342	0.02327	0.02341
		30	0.02317	0.02276	0.02217	0.02332	0.02347	0.02332	0.02346
	10	10	0.02357	0.02321	0.02268	0.02374	0.02391	0.02374	0.02390
		20	0.02362	0.02327	0.02275	0.02379	0.02396	0.02379	0.02395
		30	0.02367	0.02332	0.02282	0.02385	0.02402	0.02384	0.02400
μ_0=μ_1=4, l=2	5	10	0.01544	0.01523	0.01492	0.01556	0.01568	0.01555	0.01567
		20	0.01552	0.01531	0.01502	0.01563	0.01576	0.01563	0.01575
		30	0.01559	0.01540	0.01511	0.01572	0.01584	0.01571	0.01583
	10	10	0.01618	0.01606	0.01587	0.01633	0.01648	0.01633	0.01647
		20	0.01625	0.01614	0.01596	0.01641	0.01656	0.01640	0.01655
		30	0.01633	0.01622	0.01605	0.01648	0.01664	0.01648	0.01663